Calcif Tissue Int (1998) 63:482–489

Calcified Tissue International

Power Spectral Analysis of Vertebral Trabecular Bone Structure from Radiographs: Orientation Dependence and Correlation with Bone Mineral Density and Mechanical Properties

J. Millard, P. Augat, T. M. Link,* M. Kothari, D. C. Newitt, H. K. Genant, S. Majumdar**

Box 1290 Magnetic Resonance Science Center, Department of Radiology, 1 Irving Street, AC109, University of California, San Francisco, California 94143, USA

Received: 8 July 1997 / Accepted: 11 May 1998

Abstract. Trabecular bone structure and bone density contribute to the strength of bone and are potentially important in the study of osteoporosis. Fourier transforms of the textural patterns in radiographs of trabecular bone have previously been used for the measurement of trabecular bone structure in subjects, however, the relationship between these measures and biomechanical properties of bone have not previously been established. In this study radiographs were acquired of 28 cubic specimens of spinal trabecular bone along each of the three anatomic axes: cranio-caudal or superior-inferior (SI), medial-lateral (ML), and anterior-posterior (AP). The radiographs were digitized, background corrected, and uniformly aligned. The Fast Fourier transform (FFT) was performed on a region comprised solely of trabecular bone for each image. The zero (DC), first (FMO), and second moments (SMO) of the Fourier power spectrum and the fractal dimension (FD) as determined from the Fourier power spectrum were correlated with stereology measures, with bone mineral density (BMD) as well as with measured biomechanical properties [Young's elastic modulus (YM) and ultimate strength] of the cubes. The results show that the power spectra-based measures, when compared with structural parameters determined using 3D stereology, show good correlations with bone volume fraction, trabecular spacing, thickness, and number. These power spectral measures showed fair to good correlations with BMD and the biomechanical properties. Moreover, the correlations between the power spectral measures of trabecular structure and the BMD, YM, and stereology measures of structure depend on the orientation of the radiographic image. Specifically, these were significant differences in the measured biomechanical properties and the power spectral measures of the trabecular structure between the SI and ML and the SI and AP directions. In addition, depending on the spatial frequency range for analysis, the fractal dimension showed opposite trends with changes in BMD and biomechanical properties. Multivariate regression models showed the correlation coefficients increasing with the inclusion of some of the power spectral measures, suggesting that FFT-based texture analysis may play a potential role in studies of osteoporosis.

**Present address:* Department of Clinical Radiology, University Hospital, Westfälische Wilhelms-Universität Münster, Germany
***Present address:* Department of Orthopedic Research and Biomechanics, University of Ulm, Ulm, Germany
Correspondence to: S. Majumdar

Osteoporosis is a widely prevalent metabolic disorder that causes the loss of both cortical and trabecular bone, increasing fracture risk for those afflicted with the disease. With the advent of new therapeutic approaches, the ability to noninvasively assess and monitor osteoporotic changes and to examine the efficacy of these treatments is needed. Currently, bone mineral density (BMD) is used as the standard noninvasive tool in the evaluation of skeletal status; however, as it is not the only factor contributing to bone strength, BMD measures alone do not accurately explain fracture risk nor do they entirely reflect response to therapy [1, 2]. Because osteoporosis causes changes in the spatial distribution of bone mass through the thinning and loss of trabeculae, investigators have proposed that trabecular bone structure may play an important role in the study of osteoporosis. It is suggested that with the integration of structural quantification into the analysis of bone strength, our ability to predict and our understanding of skeletal fragility resulting from osteoporosis may improve.

Preliminary studies have applied Power Spectra-based texture analysis to the structural quantification of trabecular bone in radiographic projections [3–5]. Power Spectral analysis utilizes the Fast Fourier Transform (FFT) to derive the spatial frequency content of a complex signal. The magnitude of the Fourier transform squared, termed the ''Power Spectrum,'' can be partially characterized by its frequency moments of inertia [6]. For digitized radiographs the signal is represented by variations in pixel intensities; an image with many inter-pixel variations will contain higher frequencies than an image with uniform pixel intensities. Though radiographic depiction of trabecular bone structure pattern is a complex multidimensional parameter, some characteristics can be condensed from the power spectrum and the spectral moments of inertia. For this work we limit our analysis to the three lowest order moments: the zero (DC), the first (FMO), and the second moments of inertia (SMO). In addition, by radially averaging the power spectrum at each frequency, fractal analysis techniques may be extended to derive the fractal dimension of the trabecular pattern.

Although Calgiurli et al. [4] have shown *in vivo*, using lumbar radiographs, that power spectral analysis shows dis-

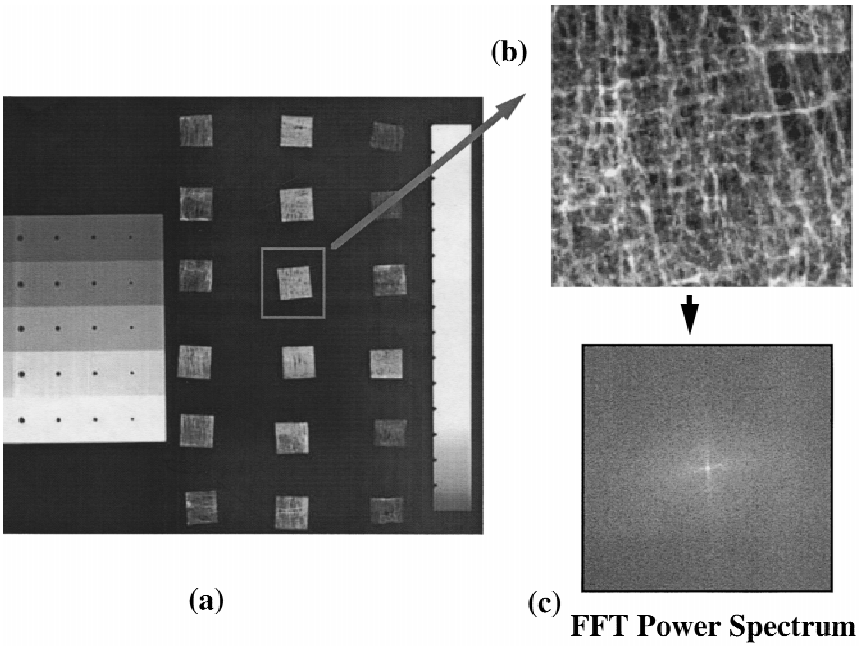

Fig. 1. (a) A radiograph of trabecular bone specimens imaged with aluminum wedges (used for standardizing image acquisition). **(b)** The digitized image of a single cube, and **(c)** its corresponding power spectrum.

crimination between patients with and without fractures, the relationship between power spectral measures of trabecular patterns in radiographs and trabecular bone structure and biomechanics has not been previously derived. Investigators have shown similar trends in discriminating osteoporotic and normal subjects using the power spectral fractal dimension [5, 7], however, the relationship among the radiographic measures, bone mechanics, and the real trabecular architecture has not been derived. It is not clear which features of trabecular architectural variations the power spectral measures from radiographs depict, or whether differences in trabecular structure in projection radiographs obtained in different orientations show the orientational and structural differences in trabecular bone. In this study, radiographic images obtained from cubes of human lumbar vertebrae were used to investigate the relationships between the structural measures represented by the moments and fractal dimension of the power spectrum and BMD, modulus of elasticity (YM), compressive strength, and actual structure parameters determined via stereology. We investigated differences in power spectral measures of trabecular architecture measured from radiographs obtained for different anatomic orientations of the cubes. Using stepwise regression models, we also investigated the ability of the power spectral measures, in addition to BMD, to predict bone strength and the elastic modulus.

Materials and Methods

Specimens

Twenty-eight trabecular bone cubes (12 mm × 12 mm × 12 mm) were cut (16 from the thoracic and 12 from the lumbar spine) from seven different cadavers using a diamond saw (EXACT, Norderstedt, Germany) under continuous irrigation. The number of samples per cadaver were not equal: there were six cubes from one cadaver, four cubes each from five cadavers, and three from one cadaver. The faces of each cube were cut as close to parallel as possible to the three anatomic axes: cranio-caudal or superior-inferior (SI), medial-lateral (ML), and anterior-posterior (AP). The region of the vertebral body from which each specimen was taken was recorded and the anatomical orientation was color-coded onto the surface of each cube using waterproof permanent ink. The specimens were then defatted first by submerging the cubes in an Alconox detergent solution and placing them in an ultrasonic cleaner for 90 minutes. Next, they were degassed by placing the specimens in distilled water for 30 minutes using a vacuum pump to free lipid lobules through the mechanical action of the displaced air. They were then submerged in 190 proof ethanol solution for 12 hours; the solution was continuously mixed. These steps were repeated 10 times or until no lipid micelles were present (however, after the first cycle, the cubes were in the Alconox detergent for only 30 minutes). Finally, the specimens were dried and radiographed, and the BMD and the biomechanical elastic modulus were determined. Following this the total number of specimens were divided into two groups: one set ($n = 19$) was used to measure compressive strength in the SI orientation, and a second set ($n = 8$) was serially sectioned and optical images were obtained in order to quantify trabecular bone architecture. The description of all these methods appears below.

Image Acquisition

Semiindustrial contact radiographs (Xomat-XTL-2, Kodak, Rochester, NY) were acquired and projected along each of the three anatomical directions using a GE DXS-350 single phase X-Ray unit (41 kVp, 125 mAs). An aluminum wedge was included in the FOV for standardization purposes, and a total of 18 cubes were X-rayed on a given film (Fig. 1). The radiographs were digitized using a laser scanner (Abe Sekkei, Inc., Tokyo, Japan) with a pixel size of 50 μm and gray level depth of 12 bits. Each specimen was cropped and stored as individual 300 × 300 pixel gray scale image files. System noise and MTF affects have been minimized in this study by standardizing film type, exposure times, and digitization protocol [8].

Image Processing

The image files were processed using a Unix work station (Sun MicroSystems, Inc.) and custom IDL (Interactive Data Language,

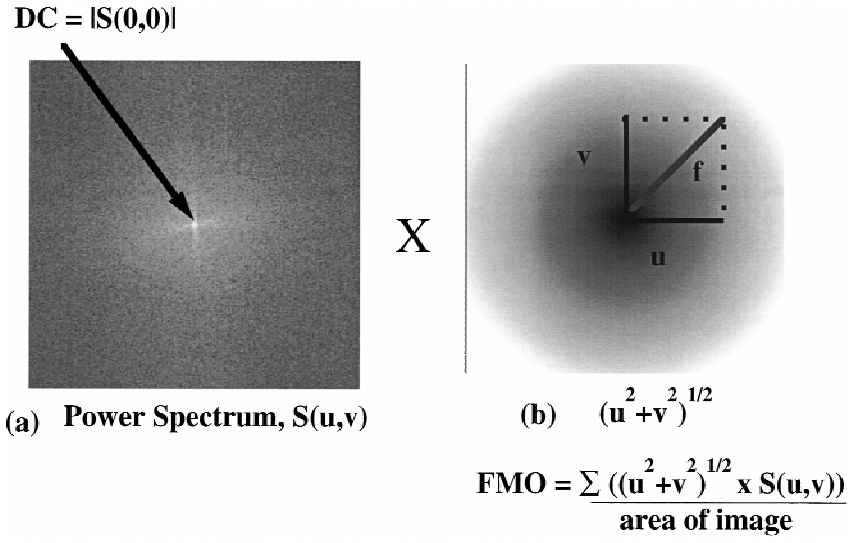

Fig. 2. The DC component, first moment (FMO) and second moment are derived from the power spectrum using Eq. 1-3. For example, the power spectrum image **(a)** is multiplied by the filter image **(b)** and intensities of the resultant image are added to produce the FMO.

Research Systems, Inc., Boulder, CO) programs. Each image was background corrected and rotated to a uniform alignment. The FFT was performed on a 9 mm × 9 mm region of interest (ROI) producing a unique two-dimensional complex array called the power spectrum (Fig. 2). The power spectrum is calculated as:

$$S(u,v) = |F(u,v)F^*(u,v)|,$$

where F(u,v) is the Fourier transform, F*(u,v) is the complex conjugate of the Fourier transform, and u and v are the spatial frequencies (number of waves per unit length) in the x- and y-directions, respectively.

Characteristic measures were calculated from the power spectrum, namely, the moments and the fractal dimension. The zero moment, also termed the ''DC component'' (DC), is the normalized power spectrum value for $u = 0$, $v = 0$. It is a measure of the average intensity of an image. The first moment (FMO) and second moment (SMO) are frequency weighted summations of the power spectrum [6, 9]:

$$DC = S(0,0)/(\text{area of image}), \quad (1)$$

$$FMO = \sum((u^2 + v^2)^{1/2} * S(u,v))/(\text{area of image}), \quad (2)$$

$$SMO = \sum((u^2 + v^2) * S(u,v))/(\text{area of image}). \quad (3)$$

The FFT-based technique for calculating fractal dimension [10] relies on the fact that the trabecular pattern is similar to a gaussian noise or stochastic process. The power spectrum, S(u,v), is converted into the polar coordinate system, such that $f = (u^2 + v^2)^{1/2}$. The values, S(f), at each given frequency, (f), are averaged over all angular distributions (Fig. 3). The power spectral-based fractal dimension is then calculated by taking the logarithm of S(f) versus log(f) curve, where the slope of the linear portion of the curve is related to FD by the equation [11, 12]:

$$FD = (7\text{-Slope})/2. \quad (4)$$

The first two frequency data points of this curve are discarded (this reduces Gibbs effect) as are the higher frequency values (done to minimize noise effects due to variations in X-ray quanta, film grain, etc.). On examining the logarithmic plot (Fig. 3), two linear regions are determined from which two different fractal dimensions were calculated. The ''coarse'' slope (denoted as Fractal1) is calculated from the lower range of the linear section of the curve ($0.5 < \log(f) < 1.0$) and the ''fine'' slope (denoted as Fractal2) from the higher range ($1.0 < \log(f) < 1.5$). The fractal dimension of trabecular bone ranges from 2.5 to 3.5 and, because the basis of this analysis is statistical, may not be equal to that measured using other fractal analysis methods [13–15].

Bone Mineral Density

BMD was determined by quantitative computed tomography (QCT), using a General Electric (Milwaukee, WI) 9800 Scanner. Five millimeter-thick slices were obtained using standardized parameters (80kVp, 140 mAs, FOV of 20 cm) and a hydroxyapatite solid calibration device (Image Analysis Inc., Columbia, KY). For each cube, a 0.8-cm^2 region of interest, located in the center of a 5 mm-thick slice was used to calculate the BMD.

Biomechanical Properties

The cubes were rehydrated in a saline solution in preparation for various biomechanical tests. Young's modulus (YM), was measured in each of the three directions from the slope of the stress-strain curve which was generated using a servo-hydraulic testing machine (MTS Bionix, Model858, Minneapolis, MN). To improve reproducibility, the specimens were preconditioned with five non-destructive cyclic compressions at a strain rate of 0.01% strain up to 5 N. Subsequently, the specimens were compressed between the lower limit of 5 N loading to 0.4% strain for three cycles. The load was measured with a precision low capacity load cell (MTS Bionix, Model 661.18C, Minneapolis, MN) and the strain was measured using an extensometer (MTS Bionix, Model 632.25F20) mounted directly across the loading plates. The raw data were recorded during all cycles and YM was determined in the last two cycles at 0.4% strain.

Also using the servo-hydraulic testing machine, 19 of the 28 specimens were destructively tested in compression in the superior-inferior direction yielding trabecular strength measures.

Stereology-Based Structure Measures

Fully automated serial grinding was used to create volumetric images of eight of the remaining bone cubes. The trabecular bone cubes were first stained black in a silver nitrate solution and then exposed to UV light. The samples were then embedded in a white pigmented methyl methacrylate polymer. A CNC milling machine serially ground each embedded specimen. After each cut, a blower and a vacuum hose were used to ensure that debris resulting from the grinding process was removed. The newly exposed surface was then imaged using a low magnification image acquistion system (consisting of a microscope and a camera with a 640 × 480 pixel resolution). After the entire specimen was ground, the 2D images were combined to form a 3D array using commercial software. The

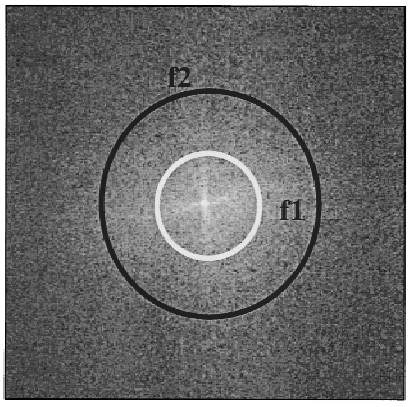

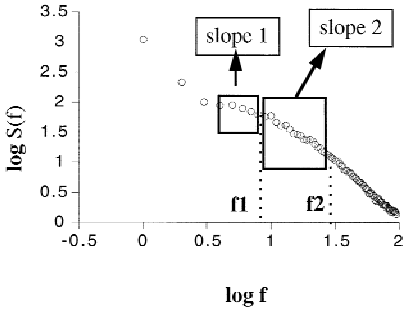

Fig. 3. To calculate fractal dimension, the sume of the power spectral values over all angular distributions is calculated for each spatial frequency (i.e., f1 and f2). The log of this summation, log S(f), is plotted as a function of the logarithm of the spatial frequency, log (f). The slopes of the linear portions of this curve can be used to determine the fractal dimension using Eq. 4.

volumetric image had an isotropic resolution of 20 μm. All the images were transferred to a remote Workstation (Sun Microsystems, Mountainview, CA) and processed using software developed in house using IDL (Interactive Data Language, Research Systems Inc. Boulder, CO). A region of interest to cover all the trabecular bone region was selected using a manual cursor. A previously documented algorithm based on the image intensity histogram was used to segment the gray level image into a binary image consisting of only a trabecular bone phase and a marrow equivalent phase [16, 17]. Three-dimensional stereological measures such as the apparent trabecular bone volume fraction, trabecular number, trabecular thickness, trabecular spacing and the mean intercept length (MIL) were computed for each image using a formulation similar to that applied to two-dimensional sections that we have previously [17] based on the definition of Parfitt et al. [18]. Details of this procedure have been previously published [17] but in summary, the segmented binary image will be used to compute the total number of bone pixels in the volume and thus compute the total bone volume fraction V_F. The total number of edges I_L between bone and marrow phases were encountered by passing a set of rays through the three-dimensional image for different angle pairs (θ, ϕ). The mean intercept as a function of angle $L(\theta, \phi)$ was calculated as $2V_FT_L/I_L$, where T_L is the total length of the lines passing through the image. Using the mean intercept lengths, the mean trabecular thickness, spacing, and trabecular number were computed for the entire volume [17].

Data Analysis

All statistical computations were done using JMP software (SAS Institute Inc., Cary, NC, USA). Relationships among the biomechanical measures, trabecular structure parameters, as well as BMD were assessed using linear regression, as well as two-tailed *t*-tests of significance and Bonferroni corrections for multiple comparisons. The contribution of having several cubes from the same cadaver was tested by examining the significance of the nominal variable, the cadaver number, when computing the linear regressions. Stepwise multiple-regression models were used to determine the combined effect of density and radiographic power spectral measures on predicting the biomechanical properties of the specimens.

Results

Radiographic projections in the SI, ML, and AP direction for one representative cube are shown in Figure 4, along with a volume-rendered image of the same cube obtained from a stack of 20 μm, optically derived images. The figure clearly depicts how a complex three-dimensional structure, when radiographically projected along different orientations, reflects the differences in trabecular structure qualitatively. In conjunction with the quantitative depiction are also quantitative differences that are apparent, as shown in Figure 5, which shows two specimens with visually different radiographic projections and the differences in the radiographic power spectral measures.

Paired *t*-tests using the Bonferroni correction for multiple comparisons showed that there were no significant differences in the measured elastic modulii (YM) between the AP and ML directions ($P < 0.9$). In comparison, there were significant differences ($P < 0.05$) between YM(SI) and YM(AP) and YM(SI) and YM(ML). These differences are most likely attributable to the fact that trabeculae form in alignment with the direction that undergoes the greatest and most frequent loading (in the case of the spine, this loading takes place in the SI direction) [19, 20]. The similarities in the YM measurements in AP and ML may be due to similar loading over time. The correlation between YM(SI) and YM(ML) and YM(SI) and YM(AP) was moderate and poor, respectively, and the correlations between the elastic modulus in the ML and AP directions was low. Although the correlation between the elastic modulus in the SI direction and strength (SI) was 0.76, it was lower between strength (SI) and the elastic modulus in ML and AP directions (Fig. 6). The influence of the individual cadavers on the correlations was tested and determined to be nonsignificant.

Using *t*-tests and the Bonferroni correction for multiple comparisons, significant differences ($P < 0.001$) were found in the power spectral measures (FMO, SMO) between the SI and the other two (ML and AP) directions, however, no differences were seen between the DC measures. The power spectral measures (FMO, SMO) between the AP and ML directions showed no significant differences. The power spectral measures and the fractal dimension in the different projections showed a range of correlations (Table 1). The DC measure showed good correlation in all directions whereas the FMO, SMO, and fractal dimension measures showed poor-to-moderate correlations, depending on the projections and parameters being compared. However, even when measured from the same projections, the correlation between the fractal measures and FMO and SMO spanned a wide range (Table 1).

To verify whether power spectral measures correspond to measures of trabecular structure, the measures were compared with standard stereology measures obtained from 20 μm serial grinding optical images: bone fraction (BV/TV), trabecular number (Tb.N), trabecular thickness (Tb.Th.), and trabecular spacing (Tb.Sp.). DC components in all pro-

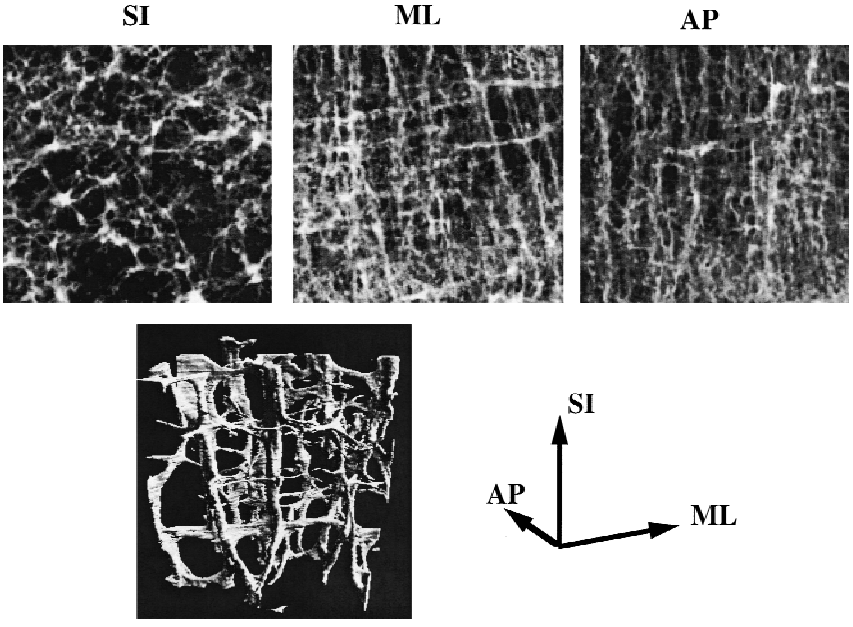

Fig. 4. A three-dimensional rendering of a representative cube is shown with the coordinates showing its orientation. For comparison, radiographs projected along the three coordinate axes, clearly depicting trabecular patterns, are also shown.

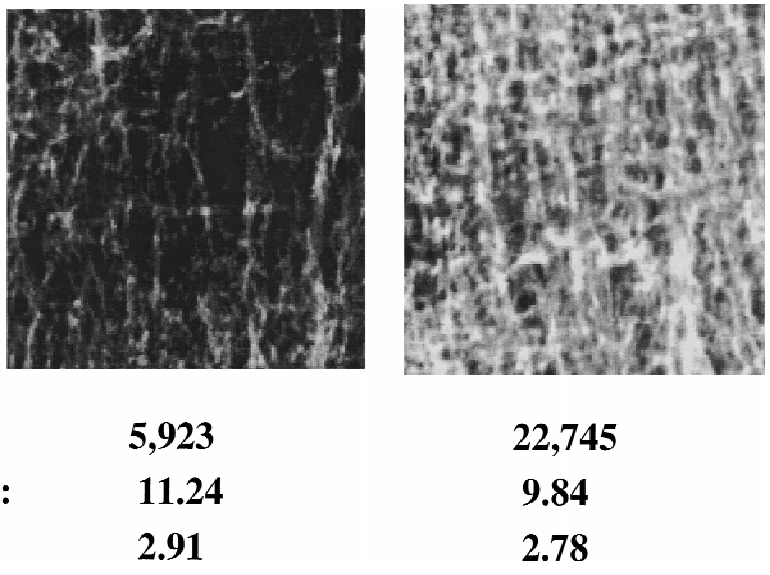

Fig. 5. Qualitative and quantitative differences in trabecular pattern are shown here for two digitized sagittal radiographs under identical image acquisiton conditions.

jections (SI, ML, and AP) were found to correlate well with bone fraction, BV/TV (R = 0.93–0.96). The results (selected ones shown in Table 2) also showed that SMO showed higher correlation with stereology measures compared with FMO; and Fractal2 correlated better than Fractal1. SMO showed good-to-excellent negative correlations with BV/TV (R = −0.76 to −0.85), Tb.N. (R = −0.80 to −0.87), and Tb.Sp. (R = 0.72–0.75); Fractal2 showed fair to good correlations with BV/TV (R = −0.73 to −0.76) and Tb.Th. (R = −0.65 to −0.82). All the correlations were significant ($P < 0.05$).

Having established an apparent relationship between the power spectral measures and trabecular bone structure, the measures were compared with BMD, elastic modulus, and strength. As seen in Table 3, there were excellent correlations between DC and BMD (R = 0.87–0.91), between DC and strength (SI) (R = 0.69–0.82), and between DC and YM(AP-ML) (R = 0.72–0.88), where YM(AP-ML) represents the mean of the measured elastic modulus in the AP and ML directions. The 1st and 2nd moments of the AP and ML projections correlated well with BMD and all biomechanical properties; however, of these, BMD and YM(AP-ML) showed the strongest correlation coefficients. FMO and SMO of the SI projections correlated poorly in all cases. The influence of the individual cadavers on the correlations was tested and determined to be nonsignificant. Also, note that both the FMO and SMO increased as BMD, elastic modulus, and strength decreased.

The correlations of fractal dimension with BMD and the biomechanical measures (Table 4) suggest that Fractal1 correlates better with strength, whereas, Fractal2 correlates best with BMD and elastic modulus. Interestingly, Fractal1 increases (whereas Fractal2 decreases) as BMD, elastic modulus, and strength increase.

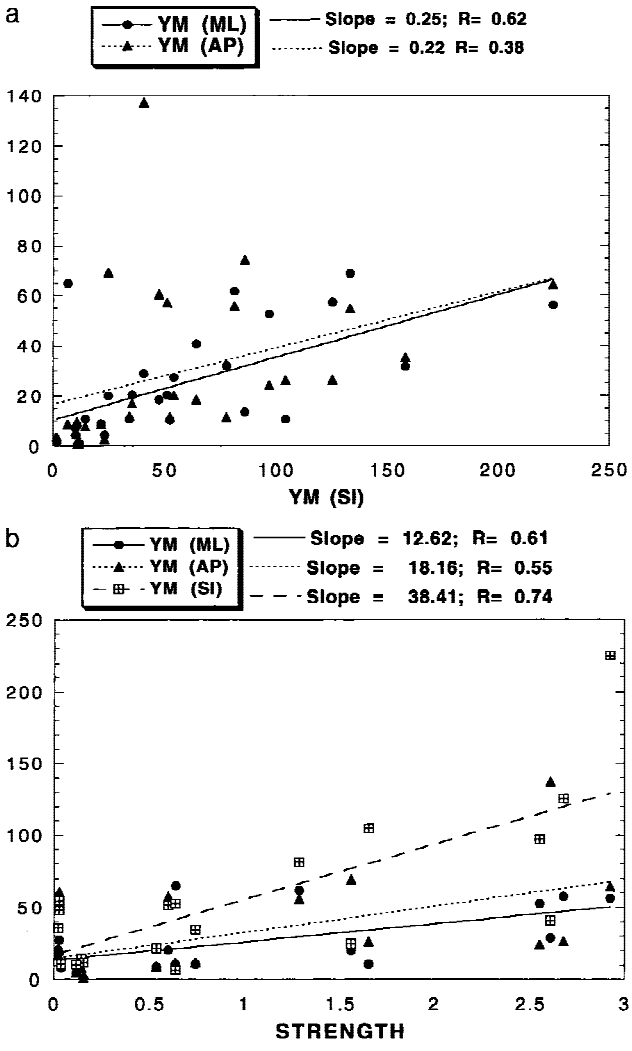

Fig. 6. (a) Correlations between elastic modulus (Modulus) in the different orthogonal directions. **(b)** Correlations between strength (SI) and modulus measures for the three anatomic directions.

Finally, a stepwise regression model was used to determine whether these power spectral and fractal dimension measures contribute to the prediction of the bone mechanics. The variables included in the model, in addition to BMD, were the power spectral measures (DC, FMO, and SMO) and the fractal dimensions (Fractal1 and Fractal2) of all three anatomic orientations. Using this model (for n = 28 specimens) for the prediction of modulus (SI), the adjusted coefficient of determination, R^2, increased from 0.42 (BMD alone) to 0.61; significant contributors ($P < 0.05$) in addition to BMD were DC(ML), SMO(AP), and DC(AP). For the prediction of modulus (AP-ML) (n = 28), the adjusted R^2 increased from 0.54 (BMD alone) to 0.83; significant ($P < 0.05$) contributors in addition to BMD were Fractal1(AP), FMO(AP) and FMO(SI). For the prediction of strength (SI) (n = 19), the adjusted R^2 increased from 0.60 to 0.91; significant contributors ($P < 0.05$) in addition to BMD were DC(ML), Fractal2(ML), Fractal1(AP), Fractal1(SI), and Fractal2(SI).

Discussion

This study indicates that radiographic images, and the im-

Table 1. Correlations between the power spectral measures (DC, FMO, SMO) and the fractal measures (Fractal1 and Fractal2) for each projection orientation (n = 28)

	DC ML	FMO ML	SMO ML	DC AP	FMO AP	SMO AP	DC SI	FMO SI	SMO SI	Fractal1 ML	Fractal2 ML	Fractal1 AP	Fractal2 AP	Fractal1 SI	Fractal2 SI	BMD
DC ML	1	−0.51	−0.63	0.83	−0.82	−0.82	0.87	−0.14	−0.42	0.30	−0.58	0.26	−0.64	0.69	−0.70	0.92
FMO ML		1	0.90	−0.51	0.52	0.47	−0.68	0.46	0.46	0.15	0.32	0.23	0.44	−0.32	0.22	−0.54
SMO ML			1	−0.63	0.60	0.68	−0.73	0.37	0.57	0.03	0.62	0.12	0.64	−0.39	0.46	−0.67
DC AP				1	−0.74	−0.76	0.89	−0.14	−0.38	0.39	−0.51	0.25	−0.59	0.66	−0.67	0.91
FMO AP					1	0.92	−0.84	0.43	0.58	−0.26	0.52	−0.20	0.62	−0.69	0.54	−0.78
SMO AP						1	−0.81	0.23	0.54	−0.34	0.74	−0.25	0.79	−0.67	0.68	−0.82
DC SI							1	−0.23	−0.41	0.30	−0.49	0.26	−0.67	0.70	−0.60	0.92
FMO SI								1	0.83	0.27	0.07	0.41	0.04	−0.06	−0.11	−0.05
SMO SI									1	−0.08	0.50	0.19	0.39	−0.30	0.34	−0.36
Fractal1 ML										1	−0.26	0.64	−0.36	0.51	−0.41	0.40
Fractal2 ML											1	−0.10	0.80	−0.37	0.77	−0.60
Fractal1 AP												1	−0.20	0.63	−0.38	0.36
Fractal2 AP													1	−0.54	0.77	−0.77
Fractal1 SI														1	−0.63	0.75
Fractal2 SI															1	−0.77
Fractal2 SI															1	−0.77

Table 2. A subset of data showing correlations between the power spectra-based measures and 3D stereology measures of volumetric images (resolution 20 %mm) (n = 8)

	BV/TV	Tb.N.	Tb.Th.	Tb.Sp.
FMO (ML)	−0.63	−0.53	−0.57	0.51
SMO (ML)	−0.82	−0.72	−0.74	0.66
Fractal1 (ML)	−0.19	−0.02	0.29	0.07
Fractal2 (ML)	−0.87	−0.62	−0.84	0.60
BMD	0.99	0.76	0.94	−0.72

Table 3. Correlations between the power spectral measures (DC, FMO, and SMO) and BMD, elastic modulus in the SI (modulus(SI)), mean elastic modulus in the AP and ML (modulus(AP-ML)), and Strength (SI)

	BMD (n = 28)	Modulus (AP-ML) (n = 28)	Modulus (SI) (n = 28)	Strength (SI) (n = 19)
DC (AP)	0.91	0.73	0.46	0.68
DC (ML)	0.92	0.75	0.69	0.80
DC (SI)	0.92	0.84	0.60	0.73
FMO (AP)	−0.81	−0.84	−0.64	−0.72
FMO (ML)	−0.51	−0.41	−0.40	−0.26
FMO (SI)	−0.08	−0.31	0.01	−0.23
SMO (AP)	−0.83	−0.80	−0.66	−0.72
SMO (ML)	−0.65	−0.56	−0.50	−0.31
SMO (SI)	−0.39	−0.50	−0.25	0.10
BMD	1.00	0.78	0.68	−0.81

Table 4. Correlations between fractal dimension (Fractal1, Fractal2) and BMD, elastic modulus in the SI (modulus(SI)), mean elastic modulus in the AP and ML, and SI

	BMD (n = 28)	Modulus (AP-ML) (n = 28)	Modulus (SI) (n = 28)	Strength (SI) (n = 19)
Fractal1 (AP)	0.38	0.47	0.30	0.73
Fractal1 (ML)	0.42	0.38	0.27	0.60
Fractal1 (SI)	0.77	0.75	0.52	0.77
Fractal2 (AP)	−0.76	−0.62	−0.61	−0.44
Fractal2 (ML)	−0.59	−0.51	−0.46	−0.32
Fractal2 (SI)	−0.77	−0.56	−0.53	−0.47
BMD	1.00	0.78	0.68	0.81

age processing techniques applied, can be used to depict orientation-dependent differences in trabecular architecture. The correlations among BMD, biomechanical properties, and the measures of trabecular bone structure derived from the power spectrum further establish the rationale for some of the *in vivo* results [4, 5, 7], indicating the valuable potential for such analysis in assessing skeletal status. Furthermore, as seen in the relationships illustrated in the correlations with the stereology measures, the power spectral measures do seem to relate to actual structural parameters.

More interesting, however, were the trends of the relationships among the fractal dimensions, BMD, elastic modulus, and strength. FFT-based fractal dimension of trabecular structure in radiographs has been the focus of various reports. One such study reported an increase in fractal dimension after alveolar bones had undergone acid-induced demineralization [7]. The same study claimed that the fractal dimension of alveolar bone images was higher in a group of postmenopausal women than a younger control group. A second study reported immobilized rat limbs to have higher fractal dimension than normal rat limbs [3]. Our study is in agreement with these earlier studies in that we found fractal dimension to be a good indicator of BMD and strength (SI), both of which are intuitively linked to structural integrity. However, our study also illustrates that fractal dimension, and its relationship to BMD and SI, ultimately depends upon the range of frequencies used; Fractal1 increases, whereas Fractal2 decreases, as BMD, elastic modulus, and strength decrease. Also, with no explaination for its cause, we found another discrepency between the two fractal dimensions: Fractal1 correlated better with strength and Fractal2 with BMD and elastic modulus.

More importantly, however, power spectral measures were found to complement BMD in stepwise regression models of elastic modulus and of strength. It was found that the ability to predict these properties increased with the addition of specific structural measures to BMD. However, it must be kept in mind that cranio-caudal radiographic projections are not clinically attainable *in vivo*, ruling out the possibility of using measures taken from this projection.

In conclusion, we have established the relationship among the power spectral-based measures of trabecular architecture, stereological measures of three-dimensional trabecular structure, BMD, and the prediction of bone mechanics. However, since the determination of compressive strength and stereology measures were both destructive procedures, not all specimens were available for all the different comparisons. This limits the study to some extent, however, it does provide a model that can be tested in an independent test set. As discussed above, although to some extent its utility has been investigated *in vivo*, further studies identifying the influence of radiographic image acquisition factors, body size, reproducibility, and the sensitivity of the technique, *in vivo*, are clearly warranted in order to identify the applicability of power spectral analysis techniques in large patient studies and to derive the relationships between these structural measures and fracture risk, therapeutic intervention, and skeletal status.

Acknowledgments. We acknowledge the assistance provided by Dr. Thomas Lang and Michael Grafe. This work was supported by NIH-RO1-AG-13612, NIH-KO4-AR-01903.

References

1. Greenfield MA (1992) Current status of physical measurements of the skeleton. Med Phys 19:1349
2. Parfitt AM (1987) Trabecular bone architecture in the pathogenesis and prevention of fracture. Am J Med 82(suppl 1B):68
3. Samarabandu J, Acharya R, Hausmann E, Allen K (1993) Analysis of bone X-rays using morphological fractals. IEEE Trans Med Imaging 12:466
4. Caligiuri P, Giger M, Favus M, Jia H, Doi K, Dixon L (1993) Computerized radiographic analysis of osteoporosis: preliminary evaluation. Radiology 186:471
5. Khosrovi PM, Kahn AJ, Genant HK, Majumdar S (1994) Characterization of trabecular bone structure from radiographs using fractal analysis. In: Raisz L (eds). American Society for Bone and Mineral Research. Kansas, USA, p 9

6. Bracewell R (1978) *The Fourier transform and its applications.* McGraw-Hill, New York
7. Ruttiman UE, Ship JA (1990) The use of fractal geometry to quantitate bone structure from radiographs. J Dental Res 69: 287
8. Chen J, Zheng B, Change YH, Shaw CC, Towers JD, Gur D (1994) Fractal analysis of trabecular patterns in projection radiographs: an assessment. Invest Radiol 29:624
9. Weszka JS, Dyer CR, Rosenfeld A (1976) A comparative study of testure measures for terrain classification. IEEE Trans Systems Man Cybernet SMC-6:269
10. Ruttiman U, RLW, Hazelrig J (1992) Fractal dimension from radiographs of peridental alveolar bone. Oral Surg Oral Med Oral Pathol 74:98
11. Cox BL, Wang JSY (1993) Fractal surfaces: measurement and applications in earth sciences. Fractals 1:87
12. Ruttimann UE, Webber RL, Hazelrig JB (1992) Fractal dimension from radiographs of peridental alveolar bone. A possible diagnostic indicator of osteoporosis. Oral Surg Oral Med Oral Pathol 74:98
13. Benhamou CL, Lespessailes E, Touliere D, Jacquet G, Harba R, Jennane R (1993) Fractal characterization of trabecular bone microarchitecture: interest of a maximum likelihood estimator. J Bone Miner Res 8:263
14. Caligiuri P, Giger ML, Favus M (1994) Multifractal radiographic analysis of osteoporosis. Med Phys 21:503
15. Majumdar S, Weinstein RS, Prasad RR (1993) Application of fractal geometry techniques to the study of trabecular bone. Med Phys 20:1611
16. Majumdar S, Newitt D, Jergas M, Gies A, Chiu E, Osman D, Keltner J, Keyak J, Genan H (1995) Evaluation of technical factors affecting the quantitation of trabecular bone structure using magnetic resonnance imaging. Bone 17:417
17. Majumdar S, Newitt DC, Mathur A, Osman D, Gies A, Chiu E, Lotz J, Kinney J, Genant H (1996) Magnetic resonance imaging of trabecular bone structure in the distal radius: relationship with x-ray tomographic microscopy and biomechanics. Osteoporosis Int 6:376
18. Parfitt A, Drezner M, Glorieux F, Kanis J, Malluche H, Meunier P, Ott S, Recker R (1987) Bone histomorphometry: standardization of nomenclature, symbols, and units. J Bone Miner Res 2:595
19. Martin RB (1991) Determinants of the mechanical properties of bones [published erratum in J Biomech 1992 Oct;25(10): 1251]. J Biomech 1:79
20. Goldstein SA (1987) The mechanical properties of trabecular bone: dependence on anatomic location and function. J Biomechanics 20:1055